Available online at www.sciencedirect.com

ScienceDirect

Procedia Engineering 81 (2014) 1682 – 1688

Procedia Engineering

www.elsevier.com/locate/procedia

11th International Conference on Technology of Plasticity, ICTP 2014, 19-24 October 2014, Nagoya Congress Center, Nagoya, Japan

Experimental and theoretical studies on formability of 22MnB5 at elevated temperatures by Gleeble simulator

Rong Shean Lee[a,*], Yi Kai Lin[b], Ta Wei Chien[a]

[a]*Department of Mechanical Engineering, National Cheng Kung University, No. 1, University Road, Tainan 701, Taiwan*
[b]*Iron & Steel R&D Department, China Steel Corporation, No.1, Chung-Kang Road, Siaogang District, Kaohsiung 81233, Taiwan*

Abstract

This paper, which includes an experimental analysis and theoretical predictions, presents a method to investigate the formability of high strength steel sheet 22MnB5 at elevated temperatures. In this method, two designs for tensile test specimens with laser engraving grids are developed and used to obtain the strain paths of a uniaxial tensile state and the plane strain occurring at elevated temperatures using a Gleeble simulator. On the other hand, a modified Cockcroft criterion that takes strain path into consideration is employed to predict the entire forming limit diagram. A forming limit diagram could be established as a result of using the modified Cockcroft criterion together with the limit strains obtained from the tensile tests based on two novel specimen designs. In this paper, forming limit diagrams at three strain rates and forming limit diagrams at temperatures ranging from 650ºC to 850ºC were established.

Selection and peer-review under responsibility of the Department of Materials Science and Engineering, Nagoya University

Keywords: Formability; 22MnB5; Elevated temperature; Gleeble simulator

1. Introduction

In hot stamping, homogeneous austenitization can be exploited to obtain fully martensitic transformation, which can achieve significant improvements in mechanical properties (Karbasian and Tekkaya, 2010). With a proper hot

* Corresponding author. Tel.: +886-6-275-7575 ext. 62147; fax: +886-6-235-2973.
E-mail address: mersl@mail.ncku.edu.tw

Selection and peer-review under responsibility of the Department of Materials Science and Engineering, Nagoya University
doi:10.1016/j.proeng.2014.10.213

stamping process, the strength of 22MnB5 can be enhanced to about 1500 MPa (Merklein et al., 2006). Besides its excellent mechanical properties, 22MnB5 also has outstanding processing properties in hot stamping, including formability and quenchability (Dahan et al., 2007). Recently, 22MnB5 has become an increasingly popular industrial material, and therefore, the need for formability information for 22MnB5 metal sheet is also increasing.

The forming limit diagram is the most critical information related to forming sheet metal. Forming limit diagrams are usually established using a limiting dome height test, but most of them are done at room temperature. The forming limit diagram of 22MnB5 should be made at elevated temperatures with cooling. When the experimental data are going to be adopted in a finite element simulation, the specimens should be tested at a constant critical temperature immediately after cooling. There are two approaches to using a limiting dome height test. In the first one, the testing specimen should be first austenitized and should then be cooled to the critical temperature at a sufficient cooling rate. Then, the cooled specimen should be moved to a testing machine and tested as soon as possible. In this way, the specimen will be cooled during the moving period. Worse still, a hot specimen is bound to be cooled by the punch. Therefore, an isolation pad should be placed between the specimen and the punch. However, even when adding a piece of asbestos paper with thickness of 0.8mm, there will still be a 30ºC/s temperature drop (Min et al., 2010). In the second method, a limiting dome height test machine that can control temperature is adopted, but there are still currently some problems with this approach. Even with proper design of the induction heating head, there was still a range of 40ºC difference between different areas on the specimen recorded in a study by Bariani et al. (2008).

Obviously, using a limiting dome height test to establish a high temperature forming limit diagram under isothermal conditions is not easy. Pellegrini et al. (2009) also stated that the standardization of a limiting dome height test for elevated temperature is far from being established. Therefore, in this paper, an alternative method for the purpose of conducting experiments under isothermal conditions more easily was developed to construct the forming limit diagram for 22MnB5. In this method, the Gleeble 3800 physical simulator and a modified Cockcroft criterion which takes strain path effect into consideration were adopted.

Nomenclature

$\sigma_{max.}$	Maximum principal stress
$d\bar{\varepsilon}$	Effective strain increment
ε_f	Effective strain at fracture
ρ	Strain ratio of strain path ($\rho = d\varepsilon_2/d\varepsilon_1$)
β	Strain path constant
$C_{fracture}$	Accumulated energy density constant

2. Theoretical studies and feasibility tests

2.1. Fracture criterion and the geometries of tensile specimens

This paper adopts a modified Cockcroft criterion with strain paths proposed by Zhuang (1990) to predict the forming limit diagram. The accuracy of this modified criterion has been verified through various material tests, including the forming limit diagram of metal sheet done using a limiting dome height test (Lee et al., 2012; Lee and Chien, 2014). The predicted forming limit diagrams have good agreement with experimental data so far. This modified criterion can be expressed as follows,

$$\frac{1}{(1+|\rho|)^{\beta}}\int_0^{\varepsilon_f}\sigma_{max.}d\bar{\varepsilon} = C_{fracture}\,, \tag{1}$$

where ρ and β denote the strain ratio of strain path ($\rho = d\varepsilon_2/d\varepsilon_1$) and a material constant related to strain path, respectively. $C_{fracture}$ and β are the two unknown parameters, which can be solved from the equations with two limit strains for two strain paths (Lee and Chien, 2014). When the values for $C_{fracture}$ and β are determined, a

forming limit curve can be constructed by varying the value of ρ from -1 to 1. In this paper, simple tensile tests and notched tensile tests were adopted to obtain different limit strains under different strain paths. The thickness of the testing sheet was 1.8mm. The geometries of the specimens are shown in Fig. 1. Square grids were engraved using the Nd:YAG laser on the surface of the specimens for the purpose of observing the strain changes during the test. According to Merklein et al. (2006), 22MnB5 exhibits no significant dependency on rolling direction at elevated temperatures, so the length direction of all the specimens used in this paper were along the rolling direction. After the preliminary tests, it was found that the simple tensile test specimen was not fractured at the expected region (region A), as shown in Fig. 2. After analysis, it was found that the central region of the specimen was the only region that was cooled. The temperature profiles of three different regions on the specimen are shown in Fig. 2. The lowest temperature was located in region A, which implies that the highest tensile strength also was located in region A, thereby enabling other regions to fracture. Since a simple tensile specimen is not applicable in this test, a modified tensile specimen with a pair of large radius notches was developed, as shown in Fig. 1. This specimen was found to be fractured in the central region.

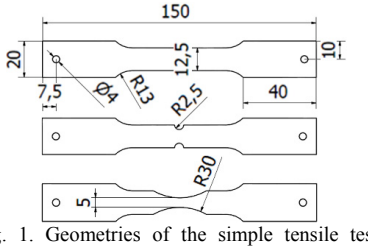

Fig. 1. Geometries of the simple tensile test specimen (up), the notched tensile test specimen (middle), and the modified specimen (bottom).

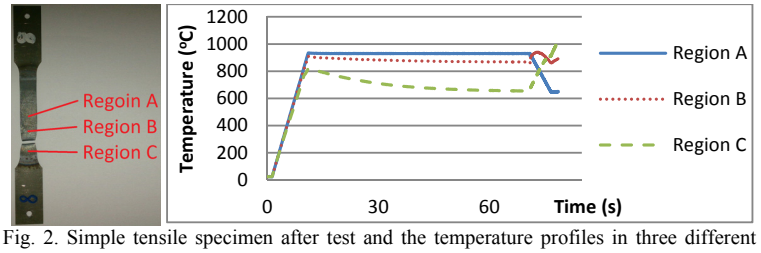

Fig. 2. Simple tensile specimen after test and the temperature profiles in three different regions.

2.2. Experimental set-up

Tensile tests at elevated temperatures can be conducted on a Gleeble 3800 physical simulator with temperature control. The temperature control system is combined with a temperature measurement system, an electrical heating system, and a jet cooling system. The temperature measurement system measures the instant temperature of the specimen through a thermocouple. According to the principles for electrical heating systems, the highest temperature always lies in the center of the specimen. Due to the configuration of the nozzles in the jet cooling system, as shown in Fig. 3, the cooling rates for different regions in a specimen are not the same. The fastest cooling rate also always lies in the center of the specimen. These two factors cause the center of a specimen to be the only region that transforms fully to martensite, which caused the failure that occurred in the preliminary tests in this study. Leaving this drawback aside, with the accuracy and the rapid responses of the thermocouple and the electrical heating system, the temperatures in the center of a specimen can be controlled within ±5ºC before cooling and within ±10ºC during cooling.

In respect to strain measurement, a high speed camera was employed to record the changes in the grids during testing. The shooting rate was set at 700 images per second. The exposure time was set at 800μs. In order to observe the strain changes during the test, the fixtures in the Gleeble 3800 were redesigned to make the surface of the specimen face toward the high speed camera, as shown in Fig. 4. The experimental setup is shown in Fig. 5.

2.3. Experimental conditions

In this paper, tension-compression limit strains and plane-strain limit strains were obtained from the modified tensile specimen and the notched specimen, respectively. Specimens were heated to 930 ºC in 10 seconds then austenitized in 60 seconds. Argon was purged into the test chamber during the test to prevent oxidation of the specimens. According to the research done by Turetta et al. (2006), the lowest cooling rate to avoid the bainitic transformation is 30ºC/s. The temperature of martensite transformation is 382 ºC. Therefore, the heated specimens were cooled at the rate of 50ºC/s and were stretched the instant they reached critical temperature under isothermal

conditions. Three different strain rates under 650 ºC were conducted, while tests under 750 and 850 ºC at similar strain rates were also performed to observe the influence of temperature. The temperature profiles during the tests at these three different critical temperatures are shown in Fig. 6.

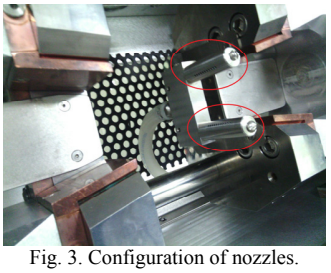

Fig. 3. Configuration of nozzles.

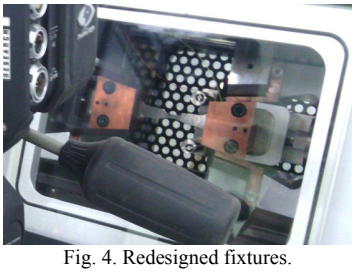

Fig. 4. Redesigned fixtures.

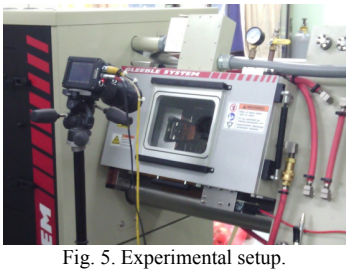

Fig. 5. Experimental setup.

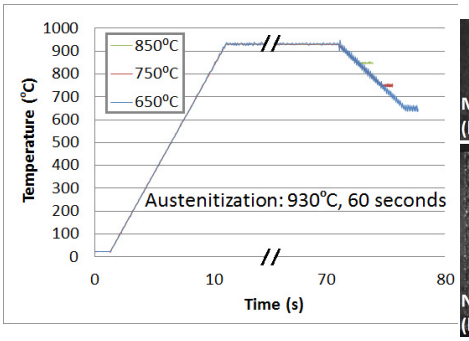

Fig. 6. Measured temperature profiles of specimens.

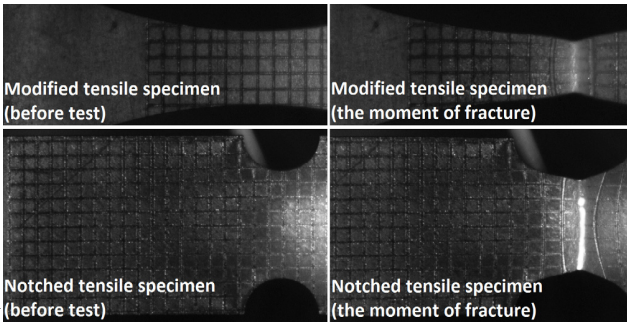

Fig. 7. The images that utilized to calculate fracture strains.

3. Results and discussion

In order to simulate an actual process, strain rates of 1/s, 3/s, and 10/s were planned. Actual local strain rates were calculated through the images with time records obtained from the high speed camera. All the local strain rates are shown in Table 1. To predict the forming limit diagram according to the modified Cockcroft criterion, in addition to the two different limit strains, the value n in Hollomon's power-law ($\bar{\sigma} = K\bar{\varepsilon}^n$) should be also obtained (Lee and Chien, 2014). Due to the fact that there was no standard tensile specimen for this experiment, an alternative was adopted. According to observations of the value adjustments, a slight change in value n only has little impact on the result for the forming limit diagram prediction, so the value n in this research was solved through the modified tensile specimen (Fig. 1). The force data and the stroke data obtained from the Gleeble 3800 were adopted as part of the information that calculated the flow stresses during the test, which are necessary data to calculate the values of n. Through the images obtained from the high speed camera, the initial length of the deformation zone was set to be 15mm, the thickness was set at 1.8mm, and the width was set at 5.5mm, respectively. The images right before fracture were selected and compared with the initial images to define the values of the fracture strains. The images used to measure the fracture strains are shown in Fig. 7. The region glowing in the notched specimen was the high temperature region that occurred at the moment of fracture.

There are currently two common ways to measure fracture strains. In the first one, the fracture strains are measured from the fractured specimens, which are taken out from the testing machine. The strains of the grids next to the fracture grids are defined as the fracture strains. The second method is digital image correlation method. In this method, the digital images of specimens during deformation are analyzed for the purpose of obtaining the

strain values on the deformed specimens, which is considered to be more accurate than the first method. The digital image correlation method was adopted in this paper, and a high speed camera with the shooting rate of 700 images per second was introduced, which is the reason why the fracture strains measured in this paper are much larger than that recorded in most of the literature for the same material and similar conditions (Pellegrini et al., 2009; Min et al., 2010; Li et al., 2013). In respect to strain rate, local strain rates can be calculated through the images with the time records obtained from the high speed camera. Strain rate was found to have little effect on the plane-strain limit strains at 650 ºC between 1 and 10 /s and the deep drawing limit strains between 1 and 3 /s, while it was shown to have significant effects on the deep drawing limit strains between 3 and 10 /s. On the other hand, according to the predicted forming limit curves, there is a downward curve in the first quadrant of forming limit diagram when the strain rate is between 1 and 3 /s, while there is an upturned curve in the first quadrant of forming limit diagram when the strain rate is 10 /s. The experimental data and the predicted forming limit diagram at 650 ºC under the three different strain rates are shown in Fig. 9. The value of the strain rate sensitivity m in the equation $\sigma = C(\dot{\varepsilon}/\dot{\varepsilon_0})^m$ under 650ºC was 0.145. The power regression line of σ and $\dot{\varepsilon}/\dot{\varepsilon_0}$ is shown in Fig. 8.

Temperature in the expected fracture region can be controlled precisely by the Gleeble 3800 physical simulator. According to the measured fracture strains, temperature has large effect on deep drawing limit strains between 650 and 850 ºC and plane-strain limit strains between 750 and 850 ºC, while it has little effect on plane-strain limit strains between 650 and 750 ºC. On the other hand, according to the predicted forming limit diagram, there is an upturned curve in the first quadrant of forming limit diagram when the testing temperature is higher than 750 ºC. The experimental data and the predicted forming limit diagram under the three different temperatures are shown in Fig. 10. The trend of the upturn curves in the first quadrant of the forming limit diagram indicates more ductility at 750 and 850 ºC as compared with that at 650 ºC.

Table 1. Experiment conditions tested in this paper.

Condition	a	b	c	d	e
Temperature	650ºC	650ºC	650ºC	750ºC	850ºC
Local strain rate (modified tensile specimen)	1.30/s	3.48/s	10.40/s	3.78/s	4.01/s
Local strain rate (notched tensile specimen)	1.14/s	2.84/s	9.41/s	3.54/s	4.07/s

Table 2. Data used to predict forming limit diagram (same temperature, different strain rates).

Condition	a	b	c
Deep drawing strain (major strain, minor strain)	0.9683, -0.3375	0.9868, -0.3293	1.0354, -0.2380
Plane strain (major strain, minor strain)	0.8489, -0.1026	0.8337, -0.0281	0.8665, -0.0548
n in Hollomon's power law	0.3007	0.3916	0.4634

Table 3. Data used to predict forming limit diagram (different temperatures, similar strain rates).

Condition	b	d	e
Deep drawing strain (major strain, minor strain)	0.9868, -0.3293	1.0963, -0.2637	1.1456, -0.2113
Plane strain (major strain, minor strain)	0.8337, -0.0281	0.9143, -0.0700	0.9687, -0.0526
n in Hollomon's power law	0.4634	0.3011	0.2378

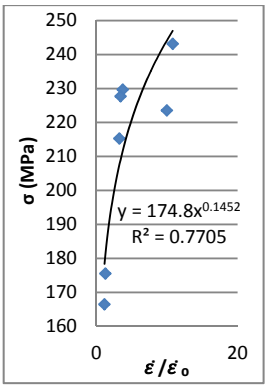

Fig. 8. Relation between σ and $\dot{\varepsilon}/\dot{\varepsilon_0}$ in 650ºC.

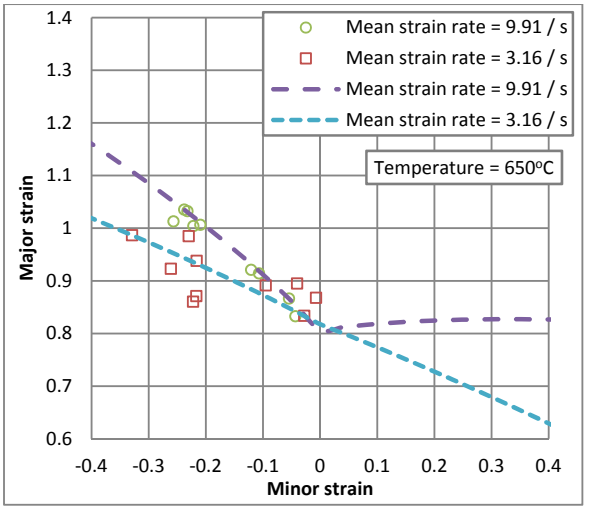

Fig. 9. Fracture strains and predicted forming limit curves at 650°C under different strain rates.

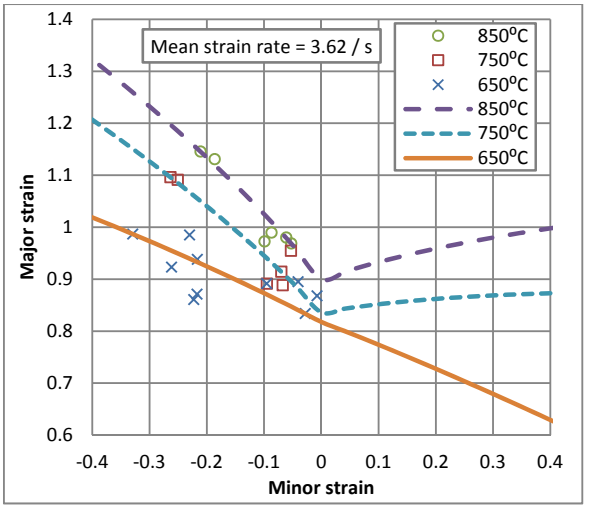

Fig. 10. Fracture strains and predicted forming limit curves at different temperatures under mean strain rates 3.62/s.

4. Conclusions and future works

An approach employing a Gleeble 3800 physical simulator and a modified fracture criterion to predict forming limit diagram in a hot stamping process was developed. In this method, forming limit curves can be predicted by the modified Cockcroft criterion together with two different tensile specimen designs. Because of the accurate temperature controlling system of the Gleeble 3800 and the new designs of the tensile specimens, the formability of a hot stamping process can be simulated more precisely. On the other hand, the images during the instant of fracture can be captured using a high speed camera, which implies more accurate data can be obtained. In addition, the images were recorded with time records, so local strain rate could also be calculated accurately. For the purposes of this paper, the effects of strain rate and temperature in the forming limit diagram of 22MnB5 metal sheet were studied. The results showed that strain rate has a significant influence on formability at strain rates larger than 3/s. The higher the strain rate is, the better the formability is. Temperature also has a significant influence on formability except under plane-strain conditions. In general, the higher the temperature is, the better the formability is. In respect to accuracy verification of the predicted forming limit curve, there are always smooth curves in both quadrants of the forming limit diagram. Therefore, tension-compression limit strains together with plane-strain limit strains are sufficient to verify the accuracy of the predicted forming limit curves in the second quadrant of the forming limit diagram, while biaxial tensile limit strains together with plane-strain limit strains are sufficient to verify the accuracy in the first quadrant. In this paper, tension-compression limit strains and limit strains close to plane-strain state were established. The predicted forming limit curves showed good agreement with the experimental data. On the other hand, the experimental limit strains in the first quadrant of the forming limit diagram are not yet established. Lee and Chien (2014) presented a biaxial tensile test performed on a cruciform tensile specimen at room temperature. The same concept potentially could be applied to hot biaxial tensile test.

Acknowledgments

The authors would like to gratefully acknowledge the China Steel Corporation in Taiwan, R.O.C. for financial support through sponsored project 102S229.

References

Karbasian, H., Tekkaya, A. E. (2010). A review on hot stamping. Journal of Materials Processing Technology, 210(15), 2103-2118.

Merklein, M., Lechler, J., Geiger, M. (2006). Characterisation of the flow properties of the quenchenable ultra high strength steel 22MnB5. CIRP Annals-Manufacturing Technology, 55(1), 229-232.

Dahan, Y., Chastel, Y., Duroux, P., Wilsius, J., Hein, P., Massoni, E. (2007). Procedure for the experimental determination of a forming limit curve for USIBOR 1500 P. In IDDRG 2007 International Conference Proceedings.

Min, J., Lin, J., Li, J., Bao, W. (2010). Investigation on hot forming limits of high strength steel 22MnB5. Computational Materials Science, 49(2), 326-332.

Bariani, P. F., Bruschi, S., Ghiotti, A., Turetta, A. (2008). Testing formability in the hot stamping of HSS. CIRP Annals-Manufacturing Technology, 57(1), 265-268.

Pellegrini, D., Lechler, J., Ghiotti, A., Bruschi, S., Merklein, M. (2009). Interlaboratory comparison of forming limit curves for hot stamping of high strength steels. Key Engineering Materials, 410, 297-304.

Zhuang, W. L. (1990). Finite element simulation for predicting the forming limit of sheet metals. Master Thesis. Department of mechanical engineering, National Cheng Kung University, Taiwan.

Lee, R. S., Chiu, H. Y., Chen, Y. J., Lo, Y. C., Wang, C. C. (2012). Evaluation of Facture Criteria Considering Complex Loading Paths in Cobalt Alloy Tube Hydroforming. Materials Transactions, 53(5), 807-811.

Lee, R. S., Chien, T. W. (2014). Formability evaluation using modified Cockcroft criterion with strain paths for sheet metal forming. Asia-Pacific Conference on Engineering Plasticity and Its Applications, AEPA 2014, Taiwan. (To appear in Key Engineering Materials)

Turetta, A., Bruschi, S., Ghiotti, A. (2006). Investigation of 22MnB5 formability in hot stamping operations. Journal of Materials Processing Technology, 177(1), 396-400.

Li, F. F., Fu, M. W., Lin, J. P., Wang, X. N. (2013). Experimental and theoretical study on the hot forming limit of 22MnB5 steel. The International Journal of Advanced Manufacturing Technology, 1-10.

Lee, R. S., Chien, T. W. (2014). A New Method for Testing Formability in sheet metal forming at Biaxial tensile state. Asia-Pacific Conference on Engineering Plasticity and Its Applications, AEPA 2014, Taiwan. (To appear in Key Engineering Materials)